Magnetic Resonance Imaging 63 (2019) 280–290

Contents lists available at ScienceDirect

Magnetic Resonance Imaging

journal homepage: www.elsevier.com/locate/mri

Original contribution

^{23}Na MRI of human skeletal muscle using long inversion recovery pulses

Tobias Wilferth[a,*], Lena V. Gast[a], Robert W. Stobbe[b], Christian Beaulieu[b], Bernhard Hensel[c], Michael Uder[a], Armin M. Nagel[a,d,e]

[a] Institute of Radiology, University Hospital Erlangen, Friedrich-Alexander-Universität Erlangen-Nürnberg (FAU), Erlangen, Germany
[b] Department of Biomedical Engineering, University of Alberta, Edmonton, Alberta, Canada
[c] Center for Medical Physics and Engineering, Friedrich-Alexander-Universität Erlangen-Nürnberg (FAU), Erlangen, Germany
[d] Division of Medical Physics in Radiology, German Cancer Research Center (DKFZ), Heidelberg, Germany
[e] Institute of Medical Physics, Friedrich-Alexander-Universität Erlangen-Nürnberg (FAU), Erlangen, Germany

ARTICLE INFO

Keywords:
Sodium (^{23}Na) MRI
Inversion recovery
Human skeletal muscle
Intracellular weighting
Long inversion pulses
B_0-inhomogeneities

ABSTRACT

^{23}Na inversion recovery (IR) imaging allows for a weighting toward intracellular sodium in the human calf muscle and thus enables an improved analysis of pathophysiological changes of the muscular ion homeostasis. However, sodium signal-to-noise ratio (SNR) is low, especially when using IR sequences. ^{23}Na has a nuclear spin of 3/2 and therefore experiences a strong electrical quadrupolar interaction. This results in very short relaxation times as well as in possible residual quadrupolar splitting. Consequently, relaxation effects during a radio-frequency pulse can no longer be neglected and even allow for increasing SNR as has previously been shown for human brain and knee. The aim of this work was to increase the SNR in ^{23}Na IR imaging of the human calf muscle by using long inversion pulses instead of the usually applied short pulses. First, the influence of the inversion pulse length (1 to 20 ms) on the SNR as well as on image contrast was simulated for different model environments and verified by phantom measurements. Depending on the model environment (agarose 4% and 8%, xanthan 2% and 3%), SNR values increased by a factor of 1.15 up to 1.35, while NaCl solution was successfully suppressed. Thus, image contrast between the non-suppressed model compartments changes with IR pulse length. Finally, *in vivo* measurements of the human calf muscle of ten healthy volunteers were conducted at 3 Tesla. On average, a 1.4-fold increase in SNR could be achieved by increasing the inversion pulse length from 1 ms to 20 ms, leaving all other parameters – including the scan time – constant. This enables ^{23}Na IR MRI with improved spatial resolution or reduced acquisition time.

1. Introduction

Since the first human *in vivo* sodium (^{23}Na) images were acquired in the 1980s [1,2], ^{23}Na magnetic resonance imaging (MRI) has advanced due to improved hardware capabilities as well as increased magnetic field strengths [3] and is nowadays established as a noninvasive technique to determine sodium concentrations in the human body. Numerous studies on sodium MRI have promised new metabolic information for many diseases such as stroke [4], tumors [5,6], multiple sclerosis [7,8] and osteoarthritis [9,10]. Besides these examples there are diseases for which not only changes in total sodium concentration, but also the separation between intra- (ICV) and extracellular volume (ECV) as well as the molecular environment of the sodium ions are of interest. Examples are hypertension [11,12] or diseases related to pathologies in the muscle such as muscular dystrophies [13–15] and channelopathies [16].

Abbreviations: J_0, J_1, J_2, spectral density parameters; $R_{2,fast}$, relaxation rate belonging to the fast component of transverse relaxation ($\omega_Q = 0$); $R_{2,slow}$, relaxation rate belonging to the slow component of transverse relaxation ($\omega_Q = 0$); $R_{2,fast,anisotropic}$, relaxation rate belonging to the fast component of transverse relaxation ($\omega_Q \neq 0$); T_{AQ}, acquisition time; $TP_{90°}$, pulse length of the 90° excitation pulse; $TP_{180°}$, pulse length of the 180° inversion pulse; T_{RO}, ADC readout time; TE, echo time; TI, inversion time; TR, repetition time; $T_{1,fast}$, relaxation time belonging to the fast component of longitudinal relaxation; $T_{1,slow}$, relaxation time belonging to the slow component of longitudinal relaxation; $T_{2,fast}$, relaxation time belonging to the fast component of transverse relaxation; $T_{2,slow}$, relaxation time belonging to the slow component of transverse relaxation; τ_c, correlation time; $\tau_{2\%}$, DQF-MA preparation time used for the xanthan 2% gel; $\tau_{3\%}$, DQF-MA preparation time used for the xanthan 3% gel; $\tau_{4\%}$, TQF preparation time used for the agarose 4% gel; $\tau_{8\%}$, TQF preparation time used for the agarose 8% gel; ω_0, lamor frequency; ω_{off}, off-resonance frequency; $\overline{\omega_Q}$, residual (time-averaged) quadrupolar splitting

* Corresponding author at: Institute of Radiology, University Hospital Erlangen, Friedrich-Alexander-Universität Erlangen-Nürnberg (FAU), Maximiliansplatz 3, 91054 Erlangen, Germany.
E-mail address: tobias.wilferth@uk-erlangen.de (T. Wilferth).

https://doi.org/10.1016/j.mri.2019.08.012
Received 3 May 2019; Received in revised form 5 July 2019; Accepted 15 August 2019

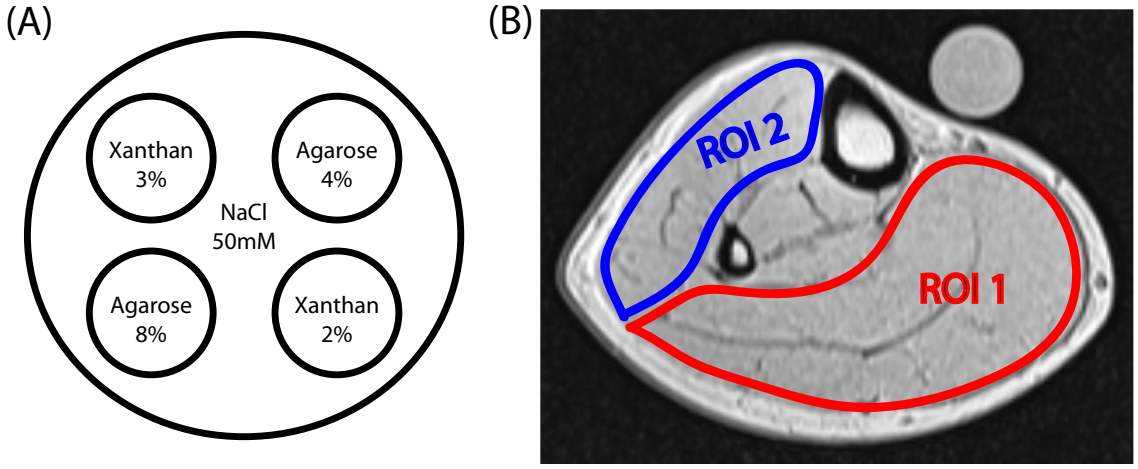

Fig. 1. The phantom used for verification of simulation results (A) consists of five compartments filled with 50 mM saline solution, agarose gel and xanthan gel. The two ROIs used for the quantitative analysis of the *in vivo* measurements (B) were chosen in a way that the two main arteries and bones were excluded. ROI1 contains the gastrocnemius lateralis, the gastrocnemius medialis and the soleus muscle and ROI2 the tibialis anterior, the peroneus longus and the extensor digitorum longus muscle.

Table 1
Spectral density parameters and residual quadrupolar splitting for the model environments at 3 T determined by fits on the signal of non-selective SE, IR, TQF and DQF FID measurements. The values are given as (mean ± standard deviation) over the five sample measurements. The relaxation times were calculated from the spectral density parameters using the relationships in [19].

	J_0 [Hz]	J_1 [Hz]	J_2 [Hz]	$\overline{\omega_Q}$ [Hz]	$T_{2,fast}$ [ms]	$T_{2,slow}$[ms]	$T_{1,fast}$ [ms]	$T_{1,slow}$ [ms]
NaCl	8.9 ± 0.1	8.9 ± 0.1	8.9 ± 0.1	–	56.0 ± 0.6	56.0 ± 0.6	56.7 ± 0.5	56.7 ± 0.5
Agarose 4%	102.6 ± 1.6	37.4 ± 1.0	13.0 ± 0.2	–	7.16 ± 0.07	19.8 ± 0.5	13.4 ± 0.4	38.5 ± 0.6
Agarose 8%	250.1 ± 1.2	45.4 ± 0.3	19.3 ± 0.3	–	3.39 ± 0.01	15.5 ± 0.1	11.0 ± 0.1	25.9 ± 0.4
Xanthan 2%	198.0 ± 2.8	22.7 ± 0.1	22.7 ± 0.2	29.3 ± 0.8	4.11 ± 0.05	–	22.1 ± 0.1	22.1 ± 0.1
Xanthan 3%	319.6 ± 1.2	28.2 ± 0.2	28.1 ± 0.2	61.8 ± 1.1	2.66 ± 0.01	–	17.8 ± 0.1	17.8 ± 0.1

In general, three different approaches have been proposed for isolating the MR signal from sodium in the ICV and therefore providing the possibility to discriminate between intra- and extracellular sodium. The first one is the use of chemical shift reagents [17], which, however, is not applicable for human *in vivo* experiments due to toxicity. A second approach is the application of multiple quantum filters, which exclusively detect the signal of sodium ions in restricted molecular environments that experience biexponential relaxation [18]. Triple quantum filters (TQF) as well as double quantum filters (DQF) have already been applied successfully in human skeletal muscle [19]. In addition, TQF techniques have already been calibrated for quantitative measurements of the intracellular sodium content in rat hearts [20,21]. However, one disadvantage of the approach is the markedly reduced signal intensity compared to a conventional spin-density weighted (SDW) acquisition [19,22,23]. The third technique is the use of IR measurements [24,25], which take advantage of considerable differences in the longitudinal relaxation between two environments in order to minimize the signal contribution from one of them. It was shown that ^{23}Na IR sequences allow for a weighting toward intracellular sodium in the human calf and, in combination with other techniques, enable an improved analysis of pathophysiological changes in muscular channelopathies [25]. The intracellular weighting is based on the differences between the sodium T_1 relaxation times in the ECV and the ICV, which are expected to exist as suggested by different shift reagent aided experiments with rats ($T_{1,ECV} \approx 40$ ms, $T_{1,ICV} \approx 20$ ms) [17,26]. It was verified for human skeletal muscle by the examination of patients with confirmed paramyotonia congenita which is characterized by a stiffening of the muscles during exercise or exposure to cold. This weakness is caused by a long-lasting depolarizing sodium inward current and the emerging elevated intracellular sodium level. In contrast to a SDW sequence, an IR sequence with an inversion time optimized for saline suppression enabled the detection of this intracellular sodium increase [25].

As a result of the strong quadrupolar interaction in spin 3/2 systems in dense macromolecular environments, sodium in general shows fast biexponential transverse and longitudinal relaxation. Therefore, when using short 180° inversion pulses with pulse lengths in the range of 1 ms, relaxation effects during the pulse cannot be completely neglected and become even more important at longer pulse lengths. As already shown for *in vivo* IR examinations of human brain [27] and knee cartilage [28], the relaxation during long inversion pulses can be used to increase the signal intensity. Furthermore, the use of inversion pulses often results in constraints concerning RF power deposition or specific absorption rate (SAR) since a 180° inversion pulse dissipates four times the power of a 90° excitation pulse. On the one hand, these problems can be mitigated by increasing the repetition time. However, this would lengthen the scan time or reduce SNR by limiting the possible number of averages in a given scan time. On the other hand, the SAR is indirectly proportional to the pulse length and therefore long inversion pulses can also be beneficial in this context.

The purpose of this work was to evaluate the application of long inversion pulses in sodium IR imaging of the human calf muscle and to evaluate the increase in SNR. This was accomplished by first determining the relaxation parameters of different model environments (saline, agarose, xanthan) in order to simulate the effects of long inversion pulses in different compartments. Here, not only SNR gain, but also image contrast and influence of B_0-inhomogeneities were examined. The simulation results were then validated by phantom measurements. Finally, the use of long inversion pulses was evaluated for *in vivo* measurements of human calf skeletal muscle. In addition to SNR, alteration of image contrast between different muscle groups with increasing length of the inversion pulse as well as the influence of B_0-

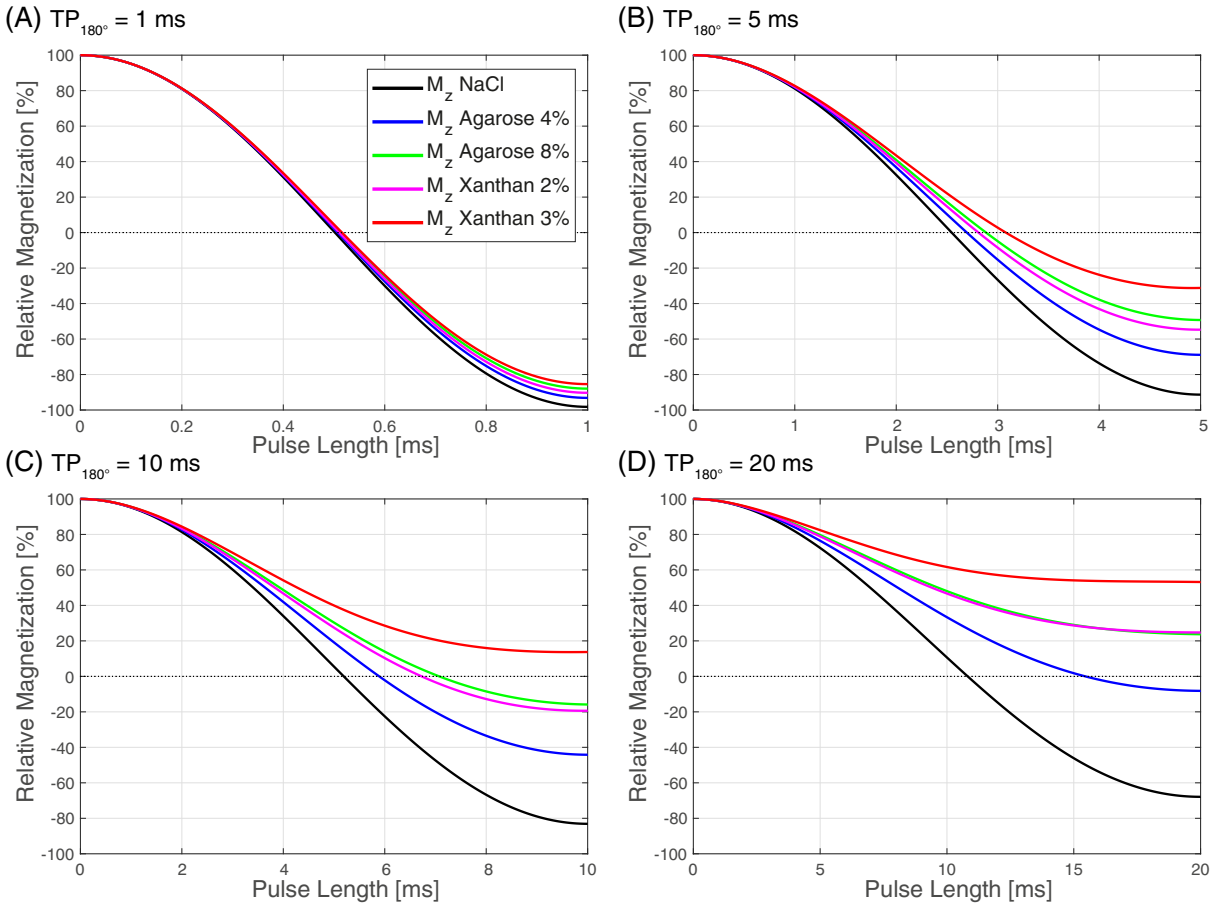

Fig. 2. Simulation results for longitudinal relaxation during 180° inversion pulses with different pulse lengths: (A) $TP_{180°}$ = 1 ms; (B) $TP_{180°}$ = 5 ms; (C) $TP_{180°}$ = 10 ms; (D) $TP_{180°}$ = 20 ms. All samples show an increase of the longitudinal magnetization at the end of the pulse and thus a decrease of the depth of the actual inversion is observed with increasing pulse length. The longitudinal magnetization of the saline solution does not recover nearly as much as the two agarose and xanthan gels at the end of longer inversion pulses. The more concentrated gels of a given type show greater differences with inversion pulse length.

inhomogeneities were investigated. The suppression of a reference phantom containing saline solution as described in [25] was examined as well.

2. Material and methods

All measurements were conducted using a 3 Tesla whole-body MR system (Magnetom Skyra, Siemens Healthineers, Erlangen, Germany) and a single-resonant birdcage knee coil (Stark Contrast, Erlangen, Germany). At the beginning of every measurement, a global flip angle calibration and a manual B_0-shim were performed. All ^{23}Na MR images were acquired using a density-adapted 3D radial readout scheme [29]. Afterwards, a custom-written Matlab tool (MATLAB, The MathWorks, Natick, MA, USA) was used to reconstruct the acquired radial raw data sets offline. A density compensation was applied before re-gridding on a Cartesian grid using a Kaiser Bessel kernel [30] with width 4.0 and an oversampling factor of 2. Image data were obtained by a Fast Fourier Transform of the re-gridded k-space data. A Hamming filter was applied to increase SNR and to reduce Gibbs' ringing artifacts [31,32].

2.1. Model environments and phantoms

In spin-3/2 systems such as ^{23}Na the spin dynamics are dominated by the interaction between the environmental electric field gradients (EFG) and the quadrupole moment of the nuclei [33]. If this interaction is static, the ^{23}Na resonance is split into three frequencies separated by the quadrupolar splitting frequency ω_Q. However, due to the thermal motion of the molecules and sodium ions in biological systems the quadrupole interaction fluctuates with time and the quadrupolar splitting frequency ω_Q is given by Eq. (1), where eq(t) is the principal value of the EFG, eQ is the electrical quadrupole moment of the nucleus and Θ denotes the polar angle between the principal value of the EFG and the B_0-field [33].

$$\omega_Q(t) = \frac{eQ}{4\hbar} eq(t)[3\cos^2\theta(t) - 1] \quad (1)$$

Within isotropic environments, the interactions are equally distributed, leading to a time-averaged – so called residual – quadrupolar splitting $\overline{\omega_Q} = 0$. In contrast, within anisotropic environments, the residual quadrupolar splitting is non-zero $\overline{\omega_Q} \neq 0$.

In the simulations as well as in the phantom measurements, three different kinds of molecular environments of ^{23}Na ions were analyzed. A saline solution with a NaCl concentration of 50 mM was used as a model for a fluid compartment ($\tau_c \ll {\omega_0}^{-1}$, $\overline{\omega_Q} = 0$). Furthermore, 4% and 8% agarose gels as well as 2% and 3% xanthan gels (Carl Roth, Karlsruhe, Germany) were produced with this saline solution. Sodium ions within agarose gel are expected to show a biexponential relaxation behavior due to the restricted mobility, but no residual quadrupolar splitting ($\tau_c \approx {\omega_0}^{-1}$, $\overline{\omega_Q} = 0$) [34,35]. Agarose gels thus represent isotropic environments. In contrast, xanthan gels have been shown to produce anisotropic environments. Above a certain threshold concentration, they develop ordered molecular structures and therefore sodium ions in xanthan gels not only show a biexponential relaxation behavior but also a residual quadrupolar splitting ($\tau_c > {\omega_0}^{-1}$, $\overline{\omega_Q} \neq 0$) [36].

In order to determine the relaxation parameters of the different

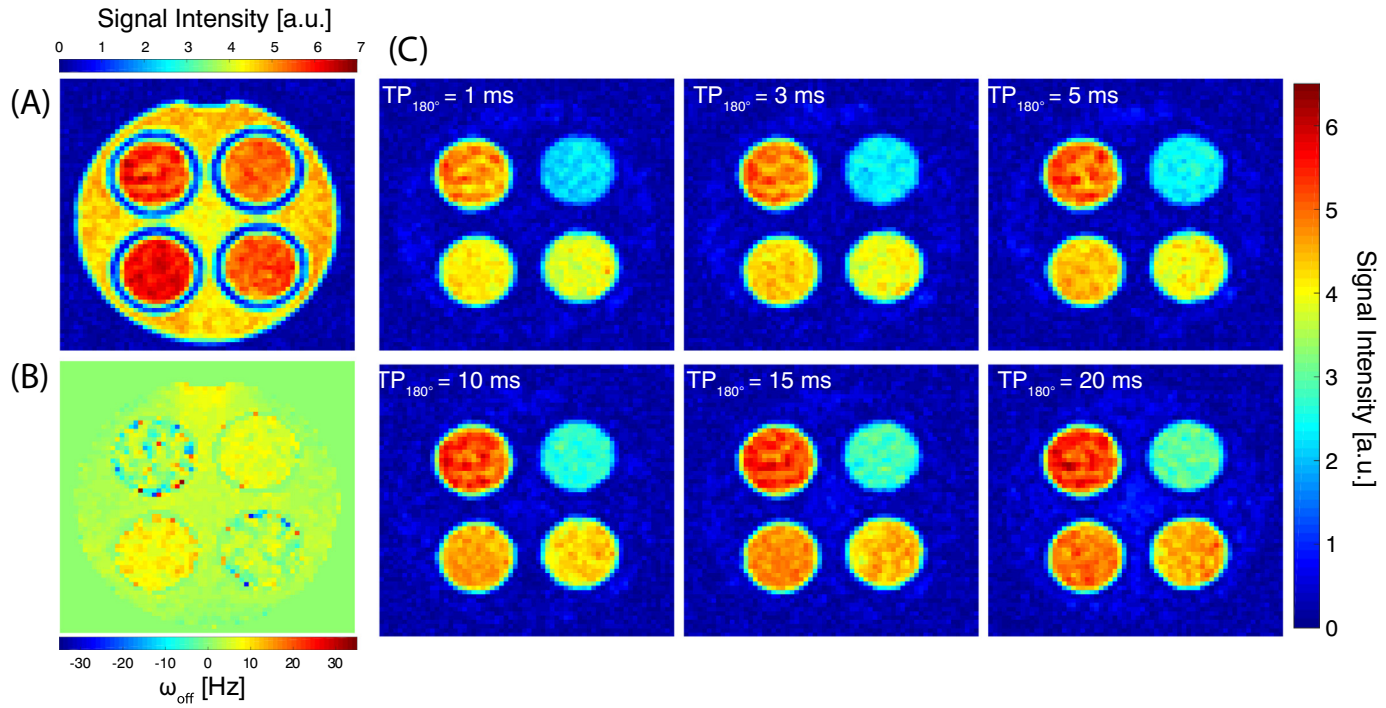

Fig. 3. Results of the phantom measurements. A SDW image (A), in which all the five compartments are visible, and the corresponding off-resonance map (B), which shows a very homogenous B_0-field over the whole phantom, are presented. All IR images of the five-compartment phantom show very good suppression of the saline solution (C). Furthermore, the expected signal increase with increasing inversion pulse length is visible in all gel compartments.

model environments, five cylindrical 1 L phantoms were produced, containing one compartment each.

In addition, a five compartment phantom was built in which all examined model compartments are available. The agarose and xanthan gels were filled in cylindrical sectors (diameter 6 cm, height 14 cm) and the space in between was filled with the saline solution (see Fig. 1A). This phantom was used to validate the simulations and to analyze the influence of B_0-inhomogeneities as well as the alteration of image contrast between the different gel compartments.

2.2. Determination of spectral density parameters and residual quadrupolar splitting

The five cylindrical one compartment phantoms were used for spatially non-selective measurements of the signal evolution of spin echo (SE) and IR as well as TQF and DQF sequences in order to determine the spectral densities $J_0 = J_0(0)$, $J_1 = J_1(\omega_0)$ and $J_2 = J_2(2\omega_0)$ and the residual quadrupolar splitting $\overline{\omega_Q}$ of the model environments. The fitting procedure directly follows from the relationships for the relaxation behavior of spin 3/2 systems described in [37]. Nonlinear least squares fitting was performed using a trust region method [38] in Matlab.

First, the spectral densities of saline solution were determined. A SE sequence with varying echo times (TE from 1 ms to 70 ms; step size: 0.5 ms for TE < 10 ms, 1 ms for TE > 10 ms) was used to analyze the transverse relaxation [see Eq. (2)]

$$s(TE) \propto \frac{3}{5} e^{-(J_0+J_1)TE} + \frac{2}{5} e^{-(J_1+J_2)TE} \tag{2}$$

and an IR sequence with varying inversion times (TI from 1 ms to 275 ms; step size: 0.5 ms for TI < 25 ms, 1 ms for TI > 25 ms) was employed to analyze the longitudinal relaxation [see Eq. (3)].

$$s(TI) \propto 1 - 2\left(\frac{1}{5} e^{-2J_1 TI} + \frac{4}{5} e^{-2J_2 TI}\right) \tag{3}$$

As all three spectral densities are expected to be equal due to the short correlation time of saline solution ($\tau_c \ll {\omega_0}^{-1}$), the mean value over all conducted measurements was used in the simulations for $J_0 = J_1 = J_2$. For the two agarose gels a slightly different approach was applied. In this case a non-selective TQF sequence (preparation time for the 4% agarose gel $\tau_{4\%} = 11$ ms and for the 8% agarose gel $\tau_{8\%} = 6$ ms for optimized signal [19]) was used to analyze the transverse relaxation [see Eq. (4)].

$$s(t) \propto e^{-R_{2,slow}t} - e^{-R_{2,fast}t} \tag{4}$$

The transverse relaxation rates are given by $R_{2,fast} = J_0 + J_1$ and $R_{2,slow} = J_1 + J_2$. To derive the remaining parameters, the longitudinal relaxation was examined using the IR sequence with variable TI. However, in this case the spectral densities are expected to have different values and, in order to obtain consistent values for the transverse and longitudinal relaxation, the relaxation rate $R_{2,slow}$ from the previous TQF measurement was used as constant parameter in the fitting process. The parameter J_1 was then determined by fitting the resulting relationship [see Eq. (5)] to the IR measurement data.

$$s(TI) \propto 1 - 2\left(\frac{1}{5} e^{-2J_1 TI} + \frac{4}{5} e^{-2(R_{2,slow}-J_1)TI}\right) \tag{5}$$

The remaining parameters were calculated from the assignments $J_0 = R_{2,fast} - J_1$ and $J_2 = R_{2,slow} - J_1$. In this approach, it was assumed that all sodium ions in an agarose sample with a certain agarose concentration have the same quadrupole interaction and therefore the phantoms were simulated using a single compartment model.

Finally, the parameters of the xanthan gels, which are the only ones expected to produce a residual quadrupolar splitting, were analyzed. Here, a DQF sequence with magic angle excitation (preparation time for the xanthan 2% and 3% gel $\tau_{2\%} = \tau_{3\%} = 1$ ms for optimized filter quality [19]) was used to determine the transverse relaxation rate and the residual quadrupolar splitting [see Eq. (6)].

$$s(t) \propto e^{-R_{2,fast,anisotropic}t} \sin(\overline{\omega_Q} t) \tag{6}$$

The relaxation rate is given by $R_{2,fast,anisotropic} = J_0 + J_1 + J_2$. The longitudinal relaxation, which is not affected by the residual

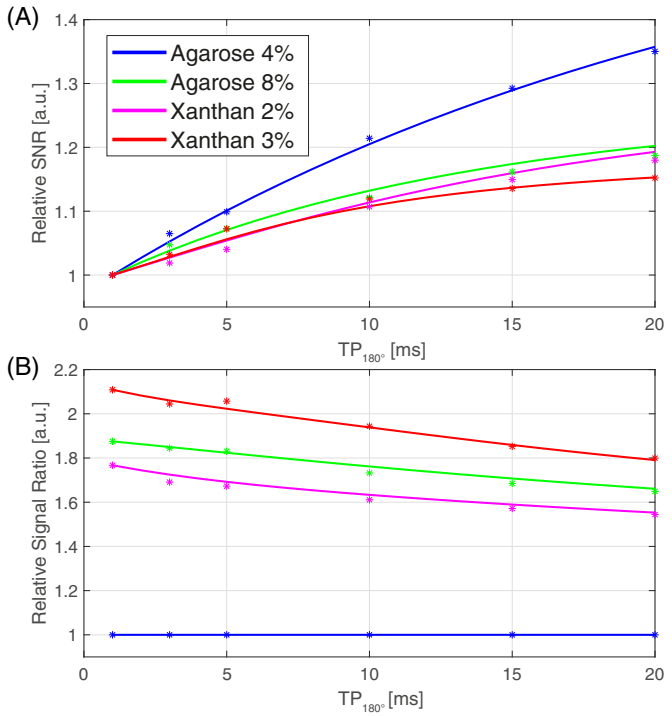

Fig. 4. The quantitative analysis of the SNR increase in the IR images (A) shows a very good agreement between simulation (lines) and measurements (stars). For all compartments a SNR gain was achieved for longer inversion pulse lengths. The slow relaxing agarose 4% compartment shows a stronger increase in signal than faster relaxing agarose 8% and xanthan compartments. The analysis of the relative signal ratio (B) also shows a very good agreement between simulation and measurements. Since the relative signal ratio of the different compartments varies with increasing inversion pulse length, image contrast between the gel compartments also depends on the used pulse length (for example agarose 4%/xanthan 3%: 2.1 at $TP_{180°} = 1$ ms and 1.8 at $TP_{180°} = 20$ ms).

quadrupolar splitting, was again examined by the IR sequence with varying TI (Eq. 3). Finally, the low-frequency spectral density parameter J_0 could easily be calculated from $J_0 = R_{2,fast,anisotropic} - J_1 - J_2$.

Every sample was measured five times in order to minimize systematic errors due to phantom position, flip angle calibration and off-resonances.

2.3. Simulations and phantom measurements

The quantum mechanical simulations of the ^{23}Na relaxation behavior during a long inversion pulse were performed with the custom-written Matlab software tool used in the work of Stobbe and Beaulieu [27]. It was designed for spin-3/2 nuclei and is based on the differential equations describing the evolution of the density operator expressed by irreducible spherical tensor operators [37,39,40]. The sequence is separated in arbitrary time intervals and for every time step the resulting matrix equation determining the spin dynamics of the systems is solved by matrix diagonalization [39]. As input parameters the spectral densities $J_0 = J_0(0)$, $J_1 = J_1(\omega_0)$ and $J_2 = J_2(2\omega_0)$ as well as a possible residual quadrupolar splitting $\overline{\omega_Q}$ were determined for the studied model environments (see Subsection 2.2).

To evaluate the relaxation behavior during long inversion pulses for each model compartment, the evolution of the longitudinal magnetization was simulated for four different inversion pulse lengths ($TP_{180°} = 1$, 5, 10 and 20 ms). Furthermore, simulations were conducted to find the optimum inversion time for suppressing the saline solution using the different inversion pulse lengths between 1 ms and 20 ms, and to determine the expected signal intensity of the non-suppressed compartments. Additionally, the influence of B_0-inhomogeneities in the range of $|\omega_{off}| \leq 60$ Hz was simulated for two inversion pulse lengths $TP_{180°} = 1$ and 20 ms.

To verify the simulation results, phantom measurements were conducted. Six IR images with different inversion pulse lengths ($TP_{180°} = 1$, 3, 5, 10, 15 and 20 ms; TI = 39 ms; TR = 300 ms; $TP_{90°} = 0.3$ ms; TE = 0.2 ms; $T_{RO} = 10$ ms; spatial resolution $\Delta x^3 = 3x3x15$ mm^3; $T_{AQ} = 51{:}02$ min for each scan) were acquired. The inversion time TI was optimized by simulations to suppress the saline compartment. The same measurements were carried out under the influence of B_0-inhomogeneities. In order to achieve this, the shim parameter ZX [41] was changed manually after shimming resulting in spatially varying off-resonances with a maximum of about $\omega_{off} = 30$ Hz.

The SNR was determined by using regions of interest (ROIs) in the different compartments as described in [42]. Since only relative SNR values were required, an additional pure noise scan was not necessary. For each compartment the relative SNR was normalized to the results of the IR sequence with inversion pulse length $TP_{180°} = 1$ ms [see Eq. (7)].

$$rSNR = \frac{signal}{signal\ (TP_{180°} = 1\ ms)} \tag{7}$$

The relative signal ratio was normalized to the measurement results of the 4% agarose gel [see Eq. (8)].

$$relative\ signal\ ratio = \frac{signal}{signal\ (agarose\ 4\%)} \tag{8}$$

As only the relative magnetization values were simulated, the simulations were normalized to the measurement results at $TP_{180°} = 1$ ms for each compartment.

2.4. In vivo measurements

Finally, *in vivo* measurements of the right human calf were performed in ten healthy volunteers (five female, five male, age 27 ± 2 years, BMI 23.5 ± 1.9). Again, six IR images with different inversion pulse lengths ($TP_{180°} = 1$, 3, 5, 10, 15 and 20 ms; TI = 34 ms; TR = 124 ms; $TP_{90°} = 0.3$ ms; TE = 0.3 ms; $T_{RO} = 10$ ms; spatial resolution $\Delta x^3 = 4x4x20$ mm^3; $T_{AQ} = 9{:}50$ min for each scan) were acquired. Transverse magnetization was spoiled using 6 ms spoiler gradients between inversion and excitation pulse. Apart from the inversion pulse length, the sequence parameters were adapted from the measurement protocol currently used in clinical studies at the institution [15] and also conform with several other muscle studies at 3 T [25,43,44]. The TI = 34 ms is optimized to suppress signal from an external saline solution reference. Studies that include patients with muscular ion channelopathies indicate that this inversion time yields a weighting toward intracellular sodium [25]. Additionally, SDW images were acquired using the first echo of a double-echo pulse sequence (TR = 120 ms; $TP_{90°} = 0.3$ ms; $TE_1 = 0.2$ ms; $TE_2 = 14$ ms; $T_{RO} = 10$ ms; spatial resolution $\Delta x^3 = 3x3x15$ mm^3; $T_{AQ} = 10{:}46$ min). In the quantitative analysis two different ROIs were used (see Fig. 1B) as earlier studies suggested that relative intensities of the DQF and TQF signals vary between different muscle groups [19]. Both ROIs were chosen in a way that the two main arteries and bones were excluded. ROI1 contains the gastrocnemius lateralis, the gastrocnemius medialis and the soleus muscle. ROI2 contains the tibialis anterior, the peroneus longus and the extensor digitorum longus muscle. Two different setups of reference phantoms were tested: The one used in clinical sodium quantification studies [15] containing four different compartments (20 mM and 40 mM NaCl solution, each with and without 4% agarose gel), which was positioned below the examined calf and a single 25 mM NaCl solution reference which was positioned above the examined calf, right next to the tibia. Two different scans were performed, one with each of the two setups.

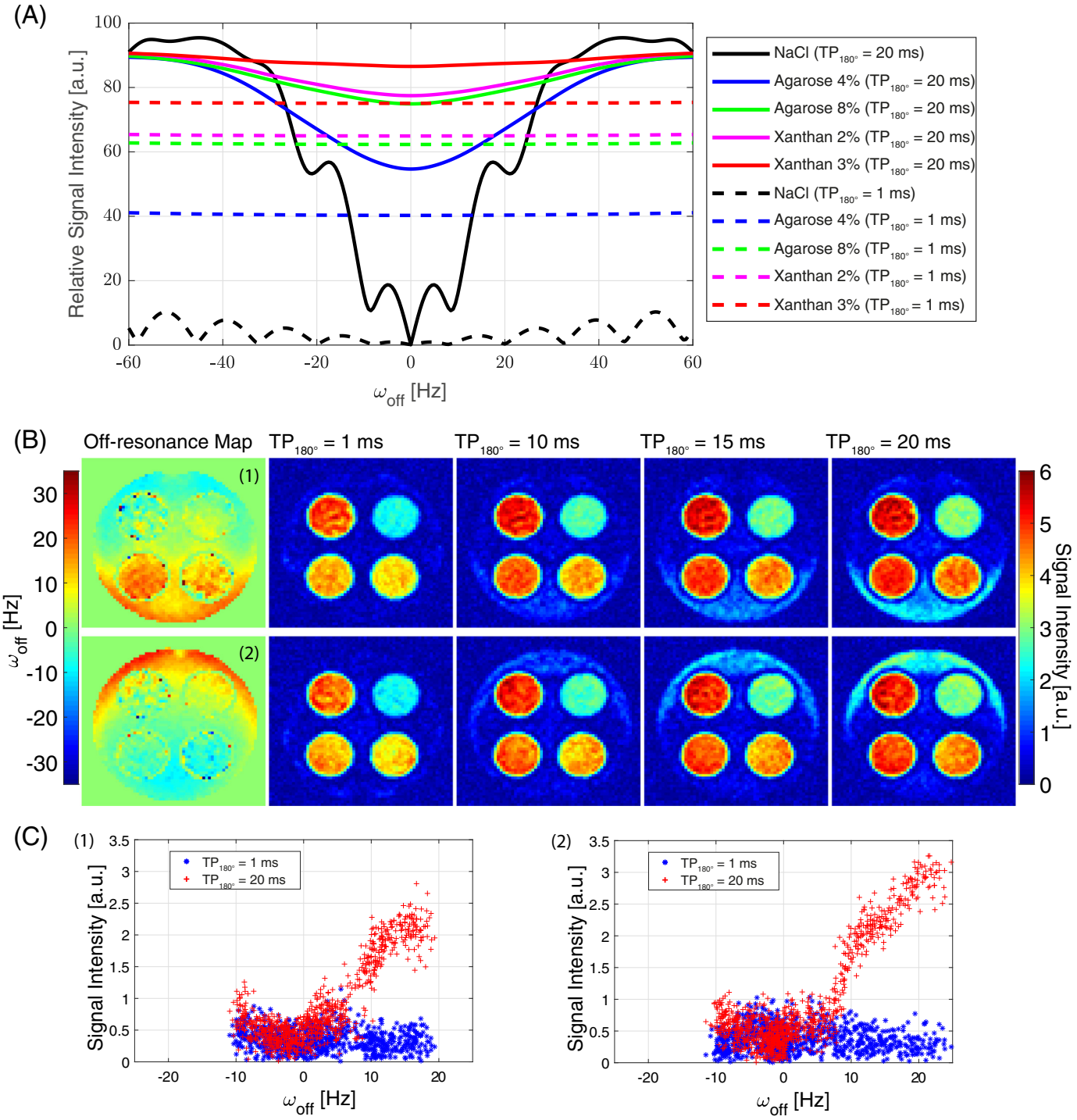

Fig. 5. Simulation (A) and measurement results (B) on the influence of B_0-inhomogeneities in IR sequences with different inversion pulse lengths. The simulations suggest that large off-resonances will deteriorate the saline suppression using long inversion pulses. This was confirmed by phantom measurements with two different orientations of applied B_0-gradients (see off-resonance maps (B1) and (B2)). In the areas with stronger off-resonances the signal of the saline solution increases with increasing inversion pulse length, in the other areas, however, the saline suppression remains similar. For short inversion pulse lengths B_0-inhomogeneities have no visible influence. The quantitative analysis of the dependency of the saline signal intensity on off-resonances (C) agrees with the simulation (A).

2.5. Determination of B_0-inhomogeneities

Additionally, to investigate the extent of B_0-inhomogeneities and to estimate their influence on the saline suppression and correspondingly the intracellular weighting in the calf, off-resonance maps were calculated from the double-echo data sets. The acquired data sets were reconstructed as complex images and the off-resonance was then given by

$$\Delta\omega = \omega_{off} = \frac{\varphi_2 - \varphi_1}{TE_2 - TE_1}, \tag{9}$$

where φ_1 and φ_2 describe the phases of each voxel of the two images corresponding to echo time TE_1 and TE_2, respectively.

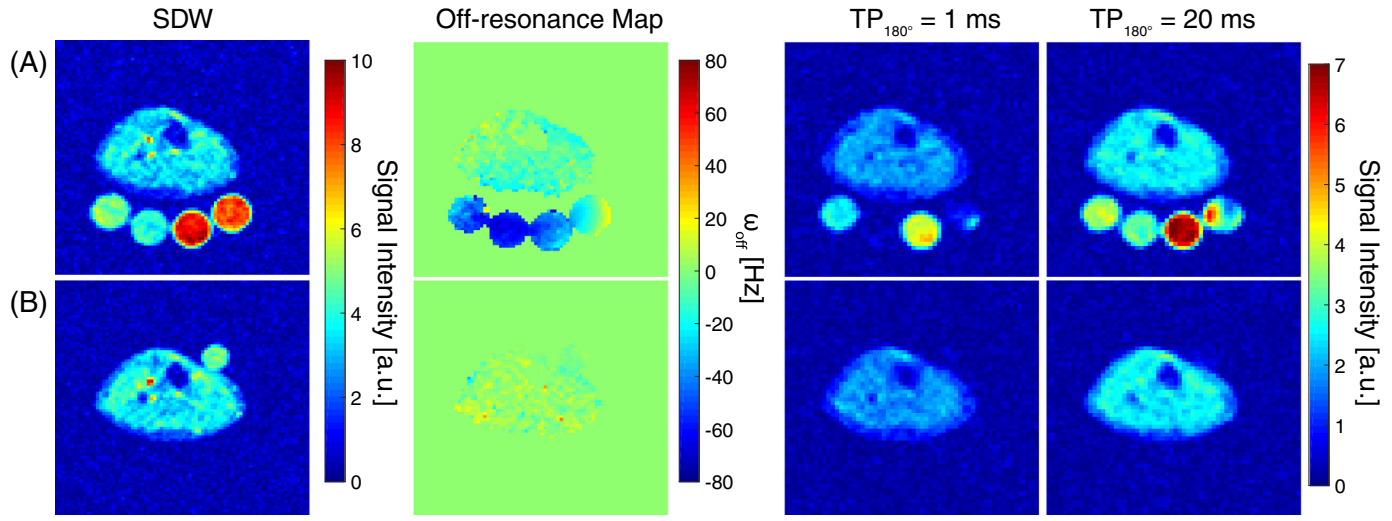

Fig. 6. SDW sodium image, off-resonance map and IR sodium images with different inversion pulse lengths for the two considered setups of references: (A) four compartments (20 mM and 40 mM NaCl solution, each with and without 4% agarose gel) as used in clinical quantification studies and (B) a single 25 mM NaCl solution reference. For setup (A), the references are off-resonant and, as a result, the saline suppression at high inversion pulse lengths was not successful. For setup (B), both the calf and the reference phantom, which is suppressed in IR images irrespective of the used inversion pulse length, are on-resonant.

Table 2
Overview of the examined volunteers as well as the corresponding results of the off-resonance measurements within the two ROIs in the calf (see Fig. 1B) and the single saline reference phantom.

Volunteer	Sex	Age [years]	BMI	Calf ω_{off} [Hz]		Reference ω_{off} [Hz]
				ROI 1	ROI 2	
1	Female	27	23.5	2.8 ± 4.6	4.4 ± 4.3	-2.1 ± 1.9
2	Female	27	21.5	1.6 ± 5.7	3.2 ± 4.5	-1.1 ± 2.2
3	Female	25	26.1	1.7 ± 4.2	3.3 ± 4.1	-13.1 ± 2.3
4	Female	24	21.5	0.0 ± 4.6	1.8 ± 6.2	-2.1 ± 2.4
5	Female	27	24.8	4.8 ± 4.0	4.7 ± 5.8	2.1 ± 1.4
6	Male	27	22.4	2.2 ± 4.4	2.4 ± 3.8	-4.5 ± 6.0
7	Male	28	23.2	6.3 ± 5.9	5.2 ± 6.6	-1.4 ± 2.5
8	Male	26	21.0	−0.5 ± 4.0	0.4 ± 5.8	0.2 ± 2.6
9	Male	24	25.7	−3.7 ± 4.9	−3.1 ± 5.3	-4.5 ± 1.6
10	Male	31	25.0	4.5 ± 5.8	2.9 ± 4.8	-1.5 ± 2.6

3. Results

3.1. Relaxation parameters

The determined spectral density parameters and the residual quadrupolar splitting as well as the corresponding relaxation times of the phantom compartments are summarized in Table 1. These values were used for all of the following simulations.

3.2. Simulations and phantom measurements

The results for the evolution of the longitudinal magnetization during 180° inversion pulses with different pulse lengths are shown in Fig. 2. For all compartments, a decrease of the degree of inversion of the longitudinal magnetization can be observed with increasing pulse length. The strength of this effect, however, depends on the actual compartment and its relaxation behavior. As a result, a clear separation of the compartments' longitudinal magnetization at the end of the inversion pulse can be achieved by elongating the pulse length.

Subsequently, the influences of these effects in IR sequences were investigated (see Fig. 3). In the SDW image all compartments are visible. The off-resonances over the whole phantom are given by ω_{off} = 3.5 Hz ± 3.9 Hz. In all IR images the signal of the saline solution is suppressed. Furthermore, the expected signal increase with increasing inversion pulse length due to relaxation effects during the pulse is visible in all non-suppressed compartments. The results of the quantitative analysis (see Fig. 4) show a good agreement between the simulations and phantom measurements. The SNR gain decreases with increasing concentration of the agarose and xanthan gels. The largest SNR gain was achieved with the 4% agarose gel. Here, a pulse length of $TP_{180°}$ = 20 ms resulted in a SNR increase of about 35% compared to a pulse length of $TP_{180°}$ = 1 ms. In the other compartments considered, signal increases varied between 15% and 22%. Irrespective of the used inversion pulse length, faster relaxing compartments provided higher signal. However, the differences in signal between the compartments decreased with increasing pulse length.

The results for the influence of B_0-inhomogeneities on IR sequences using long inversion pulses show increasing effects with longer pulse lengths (see Fig. 5). Considering the simulation results and the IR sequence with an inversion pulse length of $TP_{180°}$ = 1 ms (dashed lines), there is only a weak dependency on B_0-inhomogeneities. For an inversion pulse length of $TP_{180°}$ = 20 ms (solid lines), the B_0-inhomogeneities have a higher effect on the resulting magnetization and for off-resonances $|\omega_{off}| > 35$ Hz the saline solution even provides the highest signal. The measurement results confirm the simulation by showing that the suppression of the saline solution worsens with increasing pulse length in areas with high off-resonances.

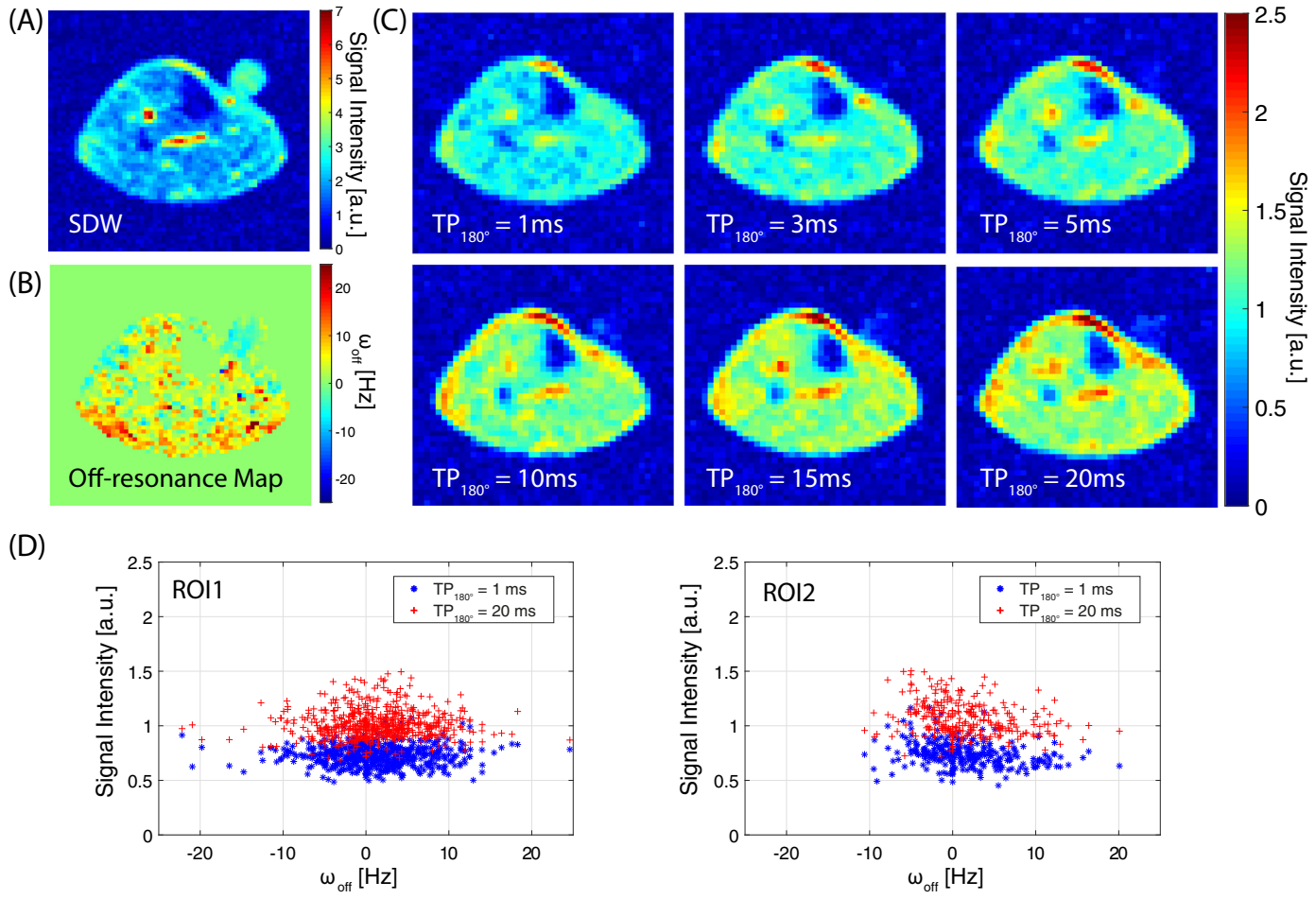

Fig. 7. Measurement results of volunteer 9 (see Table 2). In the SDW sodium image (A) the reference phantom provides signal intensity similar to that of the muscle. The off-resonance map (B) shows a homogeneous magnetic field in both the calf (ROI1: $\omega_{off} = 2.2\,Hz \pm 4.4\,Hz$; ROI2: $\omega_{off} = 2.4\,Hz \pm 3.8\,Hz$) and the reference phantom ($\omega_{off} = -4.5\,Hz \pm 6.0\,Hz$). All the sodium images of the skeletal muscle of the calf using the intracellular weighting IR sequence with different inversion pulse lengths (C) show good suppression of the saline reference phantom. Furthermore, a clear signal increase can be detected in the muscle tissue as well as in the main arteries with increasing inversion pulse length. In both examined ROIs (see Fig. 1B), no dependency of the muscle signal intensity on off-resonances has been found (D).

3.3. In vivo measurements

First, the two different setups of reference phantoms were analyzed and compared (see Fig. 6). In contrast to the single reference phantom, which does not show any off-resonances, the setup containing four different compartments shows a strong frequency shift between calf and reference. For long pulse lengths, the suppression of the saline solutions was not successful in references with strong off-resonances. As it was not possible to achieve a homogenous B_0-field using the four compartment setup the single reference was used for verification of intracellular weighting in the muscle IR experiments.

For all volunteers the B_0-homogeneity achieved within the calf was in the range where the simulation and the phantom measurements still indicated suppression of the saline solution ($|\omega_{off}| \leq 6.3 \pm 5.9\,Hz$, see Table 2). The reference phantom itself also showed a homogeneous magnetic field in all measurements. However, for one of the ten volunteers there was a relatively strong frequency shift between calf and reference, resulting in off-resonances for the latter ($\omega_{off} > 10\,Hz$). The SDW images and the off-resonance maps as well as the corresponding IR images are presented in Fig. 7 for volunteer 9 (no frequency shift) and in Fig. 8 for volunteer 3 (frequency shift). For the volunteers without frequency shift, signal originating from the reference phantom with saline solution is well suppressed, irrespective of the inversion pulse length. For the volunteer with frequency shift, the suppression of the reference decreases with increasing pulse length and vanishes completely for long pulse lengths. Both cases show a similar increase of signal in all compartments inside the calf. Here, the most notable increase can be observed in the two main arteries.

The results of the quantitative analysis of the signal increase in the calf muscle as well as the ROIs which were used are displayed in Fig. 9, exemplary for the data of volunteer 9. For all volunteers, the signal intensity in calf muscle tissue increased with increasing inversion pulse length. For the longest pulse with $TP_{180°} = 20\,ms$, approximately 1.4 times higher signal intensity could be achieved in calf muscle compared to the initial pulse length of $TP_{180°} = 1\,ms$. No significant differences were observed between the two ROIs (1.39 ± 0.05 for ROI1 and 1.41 ± 0.05 for ROI2 shown over the volunteers).

4. Discussion

In this work, the SNR of sodium IR imaging of calf tissue could be increased up to a factor of 1.4 by increasing the length of the inversion pulse and leaving all other parameters constant. Previous publications first demonstrated the corresponding sodium SNR gain in human brain [27] and knee cartilage [28] by elongating the length of the inversion pulse. Compared to 70% in brain ($TP_{180°} = 1/10\,ms$) and 120% in cartilage ($TP_{180°} = 1/24\,ms$) the achieved SNR increase of 40% in muscle seems to be low. However, in contrast to this work, in the other

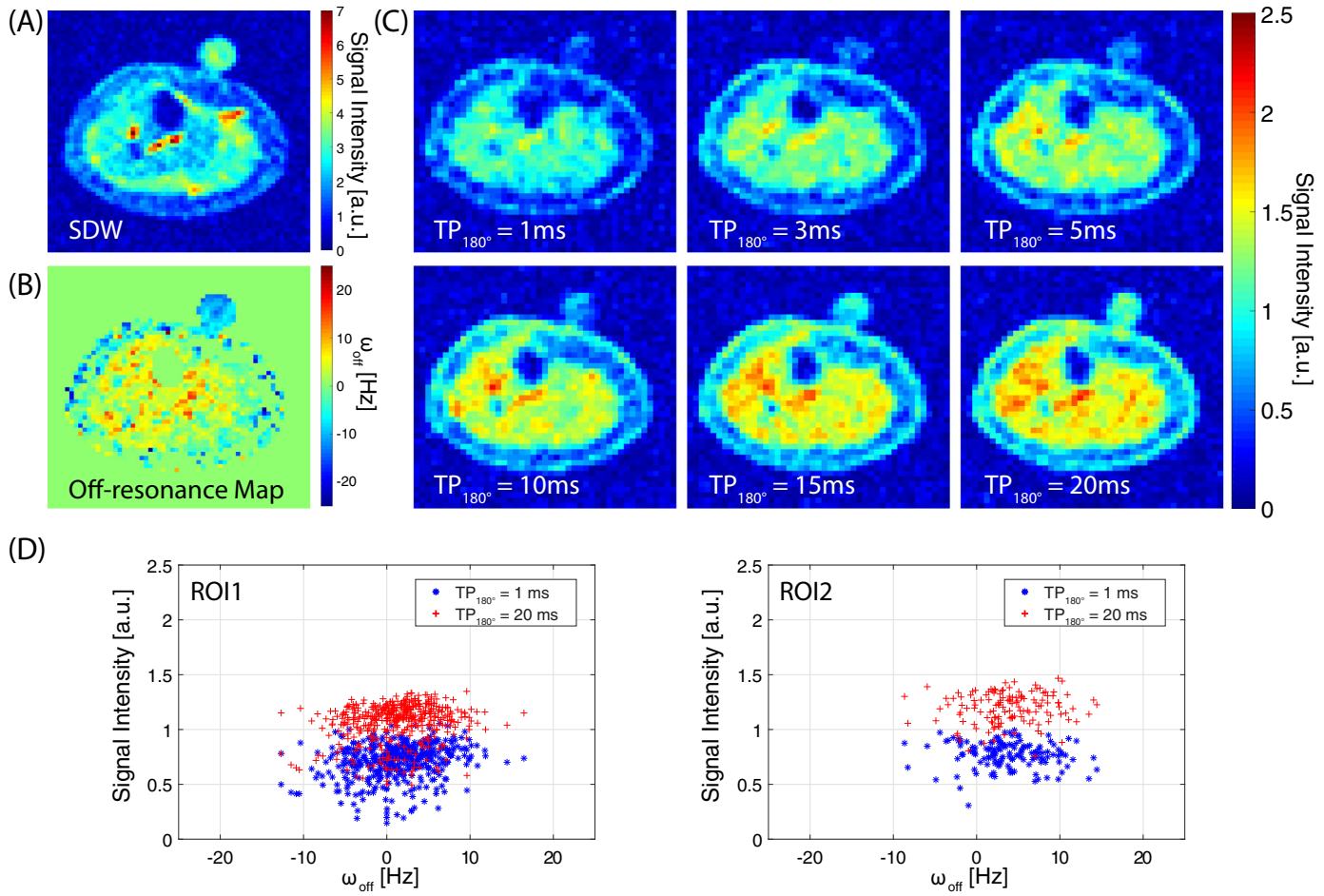

Fig. 8. Measurement results of volunteer 3 (see Table 2). In the SDW sodium image (A) the reference phantom provides signal intensity similar to that of the muscle. The off-resonance map (B) shows a frequency shift between calf and reference phantom. The magnetic field in the calf is homogenous (ROI1: ω_{off} = 1.7 Hz ± 4.2 Hz; ROI2: ω_{off} = 3.3 Hz ± 4.1 Hz), but the reference phantom shows stronger off-resonances (ω_{off} = −13.1 Hz ± 2.3 Hz). In the sodium images of the skeletal muscle of the calf using the intracellular weighting IR sequence with different inversion pulse lengths (C), the suppression of the reference phantom deteriorates as the pulse length increases. In the muscle as well as in the arteries a signal increase can be detected with increasing inversion pulse length which is comparable to the one obtained in images of volunteers with an on-resonance reference phantom (see Fig. 7). Again, in both examined ROIs (see Fig. 1B) no dependency of the muscle signal intensity on off-resonances has been found (D).

publications not only the inversion pulse length, but also other sequence parameters, in particular the repetition time and the number of averages, were optimized. In this work, we kept these parameters constant to solely analyze the influence of the increased inversion pulse length. However, an additional decrease of the repetition time and a corresponding increase of the number of averages would further improve the SNR increase. In addition, we used a relatively long inversion time of TI = 34 ms to suppress signal from saline solution. For shorter inversion times, the relaxation during the pulse has higher impact, which might lead to higher SNR increases. Furthermore, the influence of partial inversion due to relaxation also depends on the tissue sodium relaxation properties.

These dependencies when using long inversion pulses in ^{23}Na IR MRI were also observable in the performed simulations and phantom measurements. Larger percentage SNR gain could be achieved in the 4% agarose gel, which was the environment with the slowest relaxation. On the one hand, this is due to the fact that for this environment, at the initial pulse length of one millisecond, the partial inversion is only weakly pronounced, leading to a correspondingly stronger increase of relaxation effects with increasing pulse lengths. On the other hand, the faster relaxing agarose 8% and xanthan compartments already show a high signal at an inversion pulse length of 1 ms (xanthan 3%: 78% of M_0, compared to agarose 4%: 41% of M_0) due to long TI to null the saline solution. Therefore, the relative percentage increase of signal is lower. Overall, depending on the considered model environment, 1.15 to 1.35 fold higher SNR values could be achieved while saline suppression was constant.

Despite the SNR advantage, the use of longer inversion pulses has the downside of artifacts and errors due to B_0-inhomogeneities, as shown in human brain [27]. Incomplete inversion can be amplified by off-resonance, depending on the relaxation properties of the compartment. This mainly affects the saline solution, since the partial inversion recovery resulting from relaxation effects during the pulse is only weakly pronounced and stronger increased by the additional contribution due to off-resonances.

In vivo measurements of human calf muscle were performed in ten healthy volunteers. Since for the reference setup used in previous clinical ^{23}Na MRI studies (*e.g.* [45]) no homogenous magnetic field could be achieved in calf and reference at the same time, a single reference phantom was placed close to the calf and used for verification of the saline suppression in the calf muscle measurements. The reference phantom was suppressed completely in all measurements with homogeneous magnetic field (9 out of 10) even at pulse lengths of $TP_{180°}$ = 20 ms. For the measurement with strong off-resonances in the reference phantom, however, the reference signal increased with increasing pulse length. Since the setting has been chosen identically to

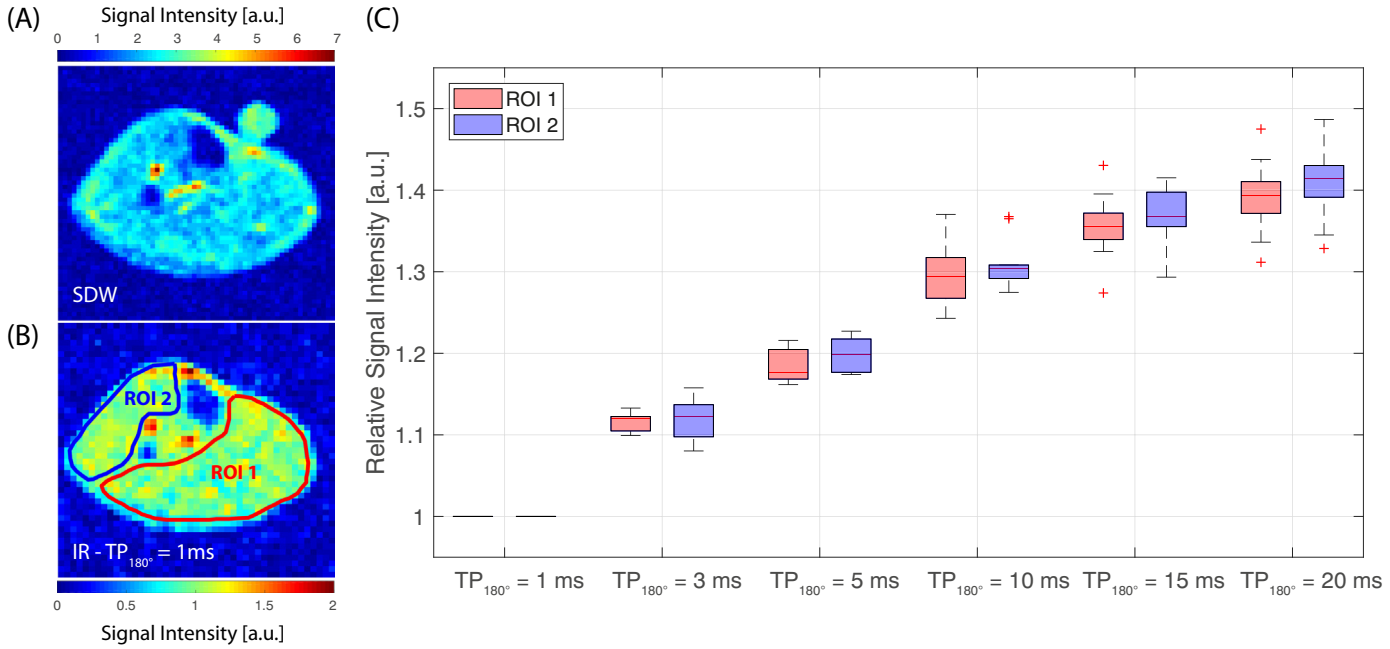

Fig. 9. (A) SDW sodium image and (B) IR sodium image with the two ROIs used to evaluate the signal increase in IR measurements with increasing inversion pulse length (volunteer 9, see Table 2). The ROIs were chosen to exclude the main arteries and bones and contain different muscle groups (see Fig. 1B). (C) All ten subjects showed an increase in signal intensity in the calf muscles with increasing inversion pulse length with no significant differences between the two ROIs (1.39 ± 0.05 for ROI1 and 1.41 ± 0.05 for ROI2 shown over the volunteers).

the other measurements, the differences in the achieved homogeneity are probably due to the anatomy of the examined subject who had considerably more subcutaneous fat compared to the other volunteers. In contrast to the off-resonances in the reference phantom mentioned above, no measurement suggested a noteworthy influence of B_0-inhomogeneities in the calf. Thus, it can be assumed that independently of the behavior of the reference phantom, B_0-inhomogeneities did not influence image quality in the area of the calf muscle. Therefore, the use of off-resonance maps is suggested to assess image quality. A correction of B_0-inhomogeneity effects during image reconstruction – as it is done for sodium SDW images [46] – might be applied to reduce image blurring. However, in addition, B_0-inhomogeneities also alter image contrast for IR imaging with long inversion pulses. A correction of this effect is challenging, since correction factors that depend on the sodium relaxation parameters would be required for each voxel. Another possibility to reduce off-resonance effects could be the use of adiabatic inversion pulses as analyzed in [47]. However, one disadvantage is the possible increase in SAR. In the conducted measurements using a 3 Tesla MR system the choice of pulse sequence parameters was not limited by SAR. However, SAR limitations are a big issue at higher field strengths, especially in IR sequences due to the 180° inversion pulse. In this context, the use of long inversion pulses will be beneficial as well, as the SAR is inversely proportional to the pulse length.

An additional investigation of the influence of B_1-inhomogeneities is not presented in detail, since the inversion pulse length has low impact on sensitivity to the effective flip angle. The results can be found in the supplementary material (see Supplementary Figure).

As already suggested by the simulations and phantom measurements, increasing the IR pulse length can also alter image contrast. In the *in vivo* calf muscle measurements, for example, the formation of a slightly different contrast between arteries and muscle could be noticed for long inversion pulse lengths. The signal of the two main arteries running through the calf showed the strongest increase with increasing pulse length, independent of subject and B_0-inhomogeneities. The main cause for the strong increase is expected to lie in the relaxation effects during the inversion pulse. Blood has a longitudinal sodium relaxation time in the range of $T_1 \approx 40–50$ ms and a considerably lower transverse sodium relaxation time ($T_2 \approx 25–35$ ms) [28,48]. Thus, it is not completely suppressed in an IR experiment with $TP_{180°} = 1$ ms and TI = 34 ms, but its signal is strongly attenuated (theoretically to about 12% - 25% of maximum signal). With longer inversion pulse lengths the importance of relaxation during the pulse increases and due to the short transverse relaxation times and the strong relaxation effects, the longitudinal magnetization at the end of the long inversion pulse increases and the attenuation thus deteriorates significantly. It should also be mentioned that whole blood has a sodium concentration of about 81 mM [48], which is higher than the one in muscle tissue, which is 15–30 mM [49]. This explains the considerably stronger signal coming from blood vessels at high pulse lengths compared to muscle tissue. In general, no significant differences between the two analyzed muscle groups were observed.

The slightly altered image contrast might also influence the extent of an intracellular weighting. The intracellular sodium is expected to have shorter transverse and shorter longitudinal relaxation times than the other compartments. For long inversion pulses, effects caused by the transverse/longitudinal relaxation should increase/decrease intracellular weighting. Thus, the resulting effect on image contrast is expected to be small and the image should still have an intracellular weighting. However, to analyze this in more detail, further examinations of patients with diseases such as paramyotonia congenital that can be used as a clinical model [25] would be required, which were not possible in this work.

5. Conclusions

In this work, the use of long inversion pulses in sodium IR images of the human calf muscle was investigated. Using an inversion pulse length of 20 ms instead of 1 ms – while keeping all other parameters constant – the SNR of IR images of calf tissue could be increased up to a factor of 1.4. No change in contrast between different muscle groups was detected. Since inside the calf the off-resonances were in a range where long inversion pulses are not susceptible to off-resonance effects, in this area the higher sensitivity of long inversion pulses to B_0-inhomogeneities was not relevant. The higher SNR might be used to

shorten the scan time or to increase the spatial resolution.

Supplementary data to this article can be found online at https://doi.org/10.1016/j.mri.2019.08.012.

Acknowledgments

We thank the Imaging Science Institute (Erlangen, Germany) for providing us with measurement time at the 3 Tesla MRI system as well as the volunteers for their participation. C.B. acknowledges the Canada Research Chair program and the Natural Science and Engineering Research Council of Canada and T.W. and A.N. the German Multiple Sclerosis Society (DMSG), V 6.2

References

[1] Hilal SK, Maudsley AA, Ra JB, Simon HE, Roschmann P, Wittekoek S, et al. In vivo NMR imaging of sodium-23 in the human head. J Comput Assist Tomogr 1985;9(1):1–7.
[2] Ra JB, Hilal SK, Oh CH, Mun IK. In vivo magnetic resonance imaging of sodium in the human body. Magn Reson Med 1988;7(1):11–22.
[3] Ladd ME, Bachert P, Meyerspeer M, Moser E, Nagel AM, Norris DG, et al. Pros and cons of ultra-high-field MRI/MRS for human application. Prog Nucl Magn Reson Spectrosc 2018;109:1–50.
[4] Tsang A, Stobbe RW, Asdaghi N, Hussain MS, Bhagat YA, Beaulieu C, et al. Relationship between sodium intensity and perfusion deficits in acute ischemic stroke. J Magn Reson Imaging 2011;33(1):41–7.
[5] Ouwerkerk R, Bleich KB, Gillen JS, Pomper MG, Bottomley PA. Tissue sodium concentration in human brain tumors as measured with 23Na MR imaging. Radiology 2003;227(2):529–37.
[6] Schepkin VD. Sodium MRI of glioma in animal models at ultrahigh magnetic fields. NMR Biomed 2016;29(2):175–86.
[7] Petracca M, Fleysher L, Oesingmann N, Inglese M. Sodium MRI of multiple sclerosis. NMR Biomed 2016;29(2):153–61.
[8] Huhn K, Engelhorn T, Linker RA, Nagel A. Potential of sodium MRI as a biomarker for neurodegeneration and neuroinflammation in multiple sclerosis. 2019. p. 10–84.
[9] Wheaton AJ, Borthakur A, Shapiro EM, Regatte RR, Akella SV, Kneeland JB, et al. Proteoglycan loss in human knee cartilage: quantitation with sodium MR imaging–feasibility study. Radiology 2004;231(3):900–5.
[10] Zbyn S, Mlynarik V, Juras V, Szomolanyi P, Trattnig S. Evaluation of cartilage repair and osteoarthritis with sodium MRI. NMR Biomed 2016;29(2):206–15.
[11] Kopp C, Linz P, Dahlmann A, Hammon M, Jantsch J, Muller DN, et al. 23Na magnetic resonance imaging-determined tissue sodium in healthy subjects and hypertensive patients. Hypertension 2013;61(3):635–40.
[12] Titze J. Water-free Na+ retention: interaction with hypertension and tissue hydration. Blood Purif 2008;26(1):95–9.
[13] Constantinides CD, Gillen JS, Boada FE, Pomper MG, Bottomley PA. Human skeletal muscle: sodium MR imaging and quantification-potential applications in exercise and disease. Radiology 2000;216(2):559–68.
[14] Weber MA, Nagel AM, Jurkat-Rott K, Lehmann-Horn F. Sodium (23Na) MRI detects elevated muscular sodium concentration in Duchenne muscular dystrophy. Neurology 2011;77(23):2017–24.
[15] Gerhalter T, Gast LV, Marty B, Martin J, Trollmann R, Schussler S, et al. (23) Na MRI depicts early changes in ion homeostasis in skeletal muscle tissue of patients with Duchenne muscular dystrophy. J Magn Reson Imaging 2019. https://doi.org/10.1002/jmri.26681.
[16] Weber MA, Nagel AM, Marschar AM, Glemser P, Jurkat-Rott K, Wolf MB, et al. 7-T (35)Cl and (23)Na MR imaging for detection of mutation-dependent alterations in muscular edema and fat fraction with sodium and chloride concentrations in muscular periodic paralyses. Radiology 2016;281(1):326.
[17] Winter PM, Bansal N. TmDOTP(5-) as a (23)Na shift reagent for the subcutaneously implanted 9L gliosarcoma in rats. Magn Reson Med 2001;45(3):436–42.
[18] Jaccard G, Wimperis S, Bodenhausen G. Multiple-quantum NMR spectroscopy of S = 3/2 spins in isotropic phase: a new probe for multiexponential relaxation. J Chem Phys 1986;85(11):6282–93.
[19] Gast LV, Gerhalter T, Hensel B, Uder M, Nagel AM. Double quantum filtered (23) Na MRI with magic angle excitation of human skeletal muscle in the presence of B0 and B1 inhomogeneities. NMR Biomed 2018;31(12):e4010.
[20] Schepkin VD, Choy IO, Budinger TF, Obayashi DY, Taylor SE, DeCampli WM, et al. Sodium TQF NMR and intracellular sodium in isolated crystalloid perfused rat heart. Magn Reson Med 1998;39(4):557–63.
[21] Schepkin VD, Choy IO, Budinger TF, Young JN, DeCampli WM. Multi-dose crystalloid cardioplegia preserves intracellular sodium homeostasis in myocardium. J Mol Cell Cardiol 1999;31(9):1643–51.
[22] Matthies C, Nagel AM, Schad LR, Bachert P. Reduction of B0 inhomogeneity effects in triple-quantum-filtered sodium imaging. J Magn Reson 2010;202(2):239–44.
[23] Tsang A, Stobbe RW, Beaulieu C. Evaluation of B0-inhomogeneity correction for triple-quantum-filtered sodium MRI of the human brain at 4.7 T. J Magn Reson 2013;230:134–44.
[24] Kline RP, Wu EX, Petrylak DP, Szabolcs M, Alderson PO, Weisfeldt ML, et al. Rapid in vivo monitoring of chemotherapeutic response using weighted sodium magnetic resonance imaging. Clin Cancer Res 2000;6(6):2146–56.
[25] Nagel AM, Amarteifio E, Lehmann-Horn F, Jurkat-Rott K, Semmler W, Schad LR, et al. 3 Tesla sodium inversion recovery magnetic resonance imaging allows for improved visualization of intracellular sodium content changes in muscular channelopathies. Invest Radiol 2011;46(12):759–66.
[26] Weidensteiner C, Horn M, Fekete E, Neubauer S, von Kienlin M. Imaging of intracellular sodium with shift reagent aided (23)Na CSI in isolated rat hearts. Magn Reson Med 2002;48(1):89–96.
[27] Stobbe R, Beaulieu C. In vivo sodium magnetic resonance imaging of the human brain using soft inversion recovery fluid attenuation. Magn Reson Med 2005;54(5):1305–10.
[28] Feldman RE, Stobbe R, Watts A, Beaulieu C. Sodium imaging of the human knee using soft inversion recovery fluid attenuation. J Magn Reson 2013;234:197–206.
[29] Nagel AM, Laun FB, Weber MA, Matthies C, Semmler W, Schad LR. Sodium MRI using a density-adapted 3D radial acquisition technique. Magn Reson Med 2009;62(6):1565–73.
[30] Jackson JI, Meyer CH, Nishimura DG, Macovski A. Selection of a convolution function for Fourier inversion using gridding [computerised tomography application]. IEEE Trans Med Imaging 1991;10(3):473–8.
[31] Stobbe R, Beaulieu C. Advantage of sampling density weighted apodization over postacquisition filtering apodization for sodium MRI of the human brain. Magn Reson Med 2008;60(4):981–6.
[32] Konstandin S, Nagel AM. Performance of sampling density-weighted and post-filtered density-adapted projection reconstruction in sodium magnetic resonance imaging. Magn Reson Med 2013;69(2):495–502.
[33] Rooney WD, Springer CS, Jr. A comprehensive approach to the analysis and interpretation of the resonances of spins 3/2 from living systems. NMR Biomed 1991;4(5):209–26.
[34] Woessner DE. NMR relaxation of spin-3/2 nuclei: effects of structure, order, and dynamics in aqueous heterogeneous systems. Concepts Magn Reson 2001;13(5):294–325.
[35] Stobbe RW, Beaulieu C. Residual quadrupole interaction in brain and its effect on quantitative sodium imaging. NMR Biomed 2016;29(2):119–28.
[36] Bezemer L, Leyte JC. Behavior of native xanthan in the biphasic region: a 23Na+ counterion NMR study. J Phys Chem 1995;99(11):3743–7.
[37] van der Maarel JRC. Thermal relaxation and coherence dynamics of spin 3/2. I. Static and fluctuating quadrupolar interactions in the multipole basis. Concepts Magn Reson Part A 2003;19A(2):97–116.
[38] Coleman TF, Li Y. An interior trust region approach for nonlinear minimization subject to bounds. SIAM J Optim 1996;6(2):418–45.
[39] Hancu I, van der Maarel JR, Boada FE. A model for the dynamics of spins 3/2 in biological media: signal loss during radiofrequency excitation in triple-quantum-filtered sodium MRI. J Magn Reson 2000;147(2):179–91.
[40] van der Maarel JRC. Thermal relaxation and coherence dynamics of spin 3/2. II. Strong radio-frequency field. Concepts Magn Reson Part A 2003;19A(2):117–33.
[41] Chang P, Nassirpour S, Henning A. Modeling real shim fields for very high degree (and order) B0 shimming of the human brain at 9.4 T. Magn Reson Med 2018;79(1):529–40.
[42] Dietrich O, Raya JG, Reeder SB, Reiser MF, Schoenberg SO. Measurement of signal-to-noise ratios in MR images: influence of multichannel coils, parallel imaging, and reconstruction filters. J Magn Reson Imaging 2007;26(2):375–85.
[43] Weber MA, Nagel AM, Wolf MB, Jurkat-Rott K, Kauczor HU, Semmler W, et al. Permanent muscular sodium overload and persistent muscle edema in Duchenne muscular dystrophy: a possible contributor of progressive muscle degeneration. J Neurol 2012;259(11):2385–92.
[44] Amarteifio E, Nagel AM, Weber MA, Jurkat-Rott K, Lehmann-Horn F. Hyperkalemic periodic paralysis and permanent weakness: 3-T MR imaging depicts intracellular 23Na overload–initial results. Radiology 2012;264(1):154–63.
[45] Kopp C, Linz P, Wachsmuth L, Dahlmann A, Horbach T, Schofl C, et al. (23)Na magnetic resonance imaging of tissue sodium. Hypertension 2012;59(1):167–72.
[46] Lu A, Atkinson IC, Claiborne TC, Damen FC, Thulborn KR. Quantitative sodium imaging with a flexible twisted projection pulse sequence. Magn Reson Med 2010;63(6):1583–93.
[47] Madelin G, Lee JS, Inati S, Jerschow A, Regatte RR. Sodium inversion recovery MRI of the knee joint in vivo at 7T. J Magn Reson 2010;207(1):42–52.
[48] Lott J, Platt T, Niesporek SC, Paech D, N GRB, Niendorf T, et al. Corrections of myocardial tissue sodium concentration measurements in human cardiac (23) Na MRI at 7 Tesla. Magn Reson Med 2019;82(1):159–73.
[49] Madelin G, Lee JS, Regatte RR, Jerschow A. Sodium MRI: methods and applications. Prog Nucl Magn Reson Spectrosc 2014;79:14–47.
[50] Morrell GR. A phase-sensitive method of flip angle mapping. Magn Reson Med 2008;60(4):889–94.